Plasma Medicine, 5(2–4): 283–298 (2015)

Mass Spectrometry Analyses of Ions Generated by Atmospheric-Pressure Plasma Jets in Ambient Air

Tomoko Ito,[1] Kensaku Gotoh,[1] Kanako Sekimoto,[2] & Satoshi Hamaguchi[1,*]

[1]Center for Atomic and Molecular Technologies, Osaka University, Suita-shi, Osaka 565-0871, Japan; [2]Yokohama City University, Kanazawa-ku, Yokohama, Kanagawa 236-0027, Japan

*Address all correspondence to: Satoshi Hamaguchi, Center for Atomic and Molecular Technologies, Osaka University, 2-1 Yamadaoka, Suita-shi, Osaka 565-0871, Japan; hamaguch@ppl.eng.osaka-u.ac.jp

ABSTRACT: For biological and medical applications of low-temperature atmospheric-pressure plasmas (APPs), gas- and liquid-phase chemical reactions caused by the plasmas determine the effectiveness of the APP-based treatments of biological systems. In this study, ions generated by helium-based low-frequency APP jets were identified by mass spectrometry. It is shown that, among all positive ions generated by plasma jets in ambient air, hydronium ions (H_3O^+) are the dominant ions that form water clusters. The stability of a hydronium ion with water molecules suggests that all positive ions generated by plasma jets would transfer their charges to hydronium ions if water molecules were abundant, such as in humid air or water. Similarly, it is shown that, among all negative ions generated by the plasma jets in ambient air, relatively few, such as OH^-, HO_2^-, NO_2^-, NO_3^-, HCO_3^-, and HCO_4^-, form water clusters stably. The densities of positive and negative ions generated in ambient air by the APP jet system, as well as the concentrations of H_2O_2 and NO_2^- generated in pure water exposed to the same plasma, have been also measured.

I. INTRODUCTION

A low-temperature atmospheric-pressure plasma (APP) is an efficient source of highly reactive species in the gas phase. Because of its nature of low gas temperature (i.e., gas temperature being close to the ambient temperature), the use of APPs to treat heat-sensitive surfaces of materials, including living tissues, for biological and medical applications such as sterilization and wound healing has been studied widely in recent years.[1–5] Although several beneficial effects of such treatments have been reported, in many cases, the causes of the effects have remained unclear.

It is widely known that chemically reactive species are generated by APPs[6–14] in ambient air. When living tissues or cells are exposed to APPs, the reactive species are first transferred to the surface of a liquid such as blood, lymph, or cell culture medium that covers the living tissues or cells. Then, the plasma-generated reactive species either continue to diffuse or are converted to different types of chemical species in the liquid and may eventually reach the tissue or cell surfaces. Interactions between the reactive species and cells are believed to trigger a complex chain of biological reactions in the system.

In this study, we examine ions generated by helium-based low-frequency APP jets

1947-5764/15/$35.00

in ambient air experimentally. The goal of this study was to identify gas-phase ions generated by the plasma system that we use routinely for various experiments.[15–19] We also compare the results with previously published mass spectrometry data obtained for different types of APP systems.

In ion mass spectrometry in ambient air, it is known that ions observed in a mass spectrometer may not be the same as those that exist in ambient air. This is because ions that enter a spectrometer typically undergo a series of rapid chemical reactions as they travel in a low-pressure region of the mass spectrometry system and collide with other gaseous species. Because of such gas-phase chemical reactions inside spectrometry systems, ion mass spectra observed for the same APP by different spectrometers are typically different. Such machine dependence of mass spectra makes it difficult to understand the gas-phase ion chemical reactions in ambient air based on mass spectrometry. In this study, we analyze ion mass spectra of APPs generated by the helium-based low-frequency APP jet system, hoping that a comparison of the obtained mass spectra with published data of earlier studies[20–23] would provide an insight into the gas-phase ion chemistry of the APP jet system.

Reactive oxygen and nitrogen species (RONS) are also generated in liquid when the liquid is subject to plasma irradiation.[18 19,24–26] In this study, we also measure the concentrations of H_2O_2 and NO_2^- generated by helium-based low-frequency APP jets in pure water as sample RONS. RONS generated in water by plasma irradiation should be closely related to gas-phase chemistry caused by the plasma.

II. EXPERIMENTAL PROCEDURE

The helium-based low-frequency APP jet system that we used in this study is the same design as the one used in the study of Miura et al., 2014[19] and similar to those used in the studies of Ando et al., 2013,[15] 2011,[16] and 2012[17] and Ikawa et al., 2010.[18] It consists of a glass tube, in which a He gas flows and two brass electrodes wound around the glass tube, as depicted schematically in Figure 1. The frequency of high-voltage power supply (PVM200) was in the range of ~20–30 kHz and the peak-to-peak voltage was varied from 6 to 12 kV. The flow rate of He gas used in this study was in the range of ~1–3 L/min. The inner and outer diameters of the glass tube for He gas flow were 1.5 and 3.0 mm, respectively, and its length was 15 cm. The gas temperature of plasma generated in this system was measured and confirmed to be close to room temperature.

Positive and negative ion densities generated by the plasma in ambient air were measured as functions of the distance from the discharge using an Ebert-type atmospheric ion counter (ITS-201A, ANDES Electric). The distance between the tip of the plasma jet and the ion counter was varied horizontally along the laboratory bench surface, as shown schematically in Figure 1.

Mass spectrometry of ions generated by the plasma system was performed using an LC-mate double-focusing mass spectrometer (JEOL, Tokyo, Japan).[27,28] The tip of the plasma jet was aligned with the center of the mass spectrometer orifice, which was 130 μm in diameter. The distance between the plasma-jet tip and the orifice was 3 mm. To

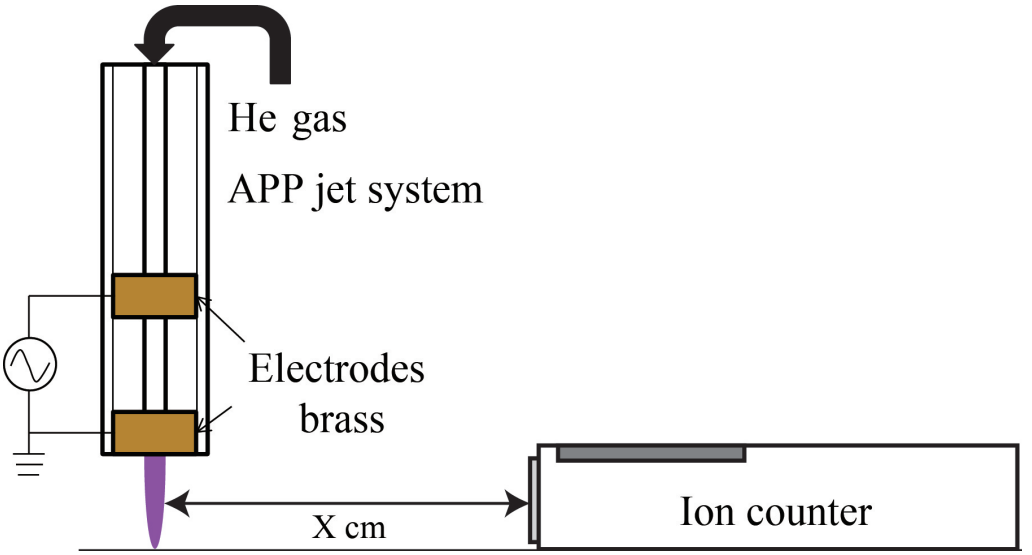

FIG. 1: Schematic diagram of ion density measurement for the helium-based low-frequency APP jet system. The distance between the plasma and the ion counter inlet was varied along the laboratory bench surface.

minimize the rise of pressure in the first differentially pumped stage of the mass spectrometer, an extra-fine tube was inserted in the orifice and the tip of the tube was bent to prevent a direct blowing of the gas from the plasma system, as shown schematically in Figure 2. The mass spectrometer used in this study can measure negative and positive ions having the mass-to-charge ratios (i.e., *m/z*) larger than 10 and 50, respectively.

The concentrations of hydrogen peroxide (H_2O_2) and NO_2^- formed in pure water were also measured by APP jet irradiation. These measurements were performed by colorimetry with 4-aminoantipyrine (for H_2O_2) and naphthyl ethylenediamine (for NO_2^-) (Kyoritsu Chemical-Check). In the experiments, 2 ml of pure water, placed in a well of a 24 well plate, was exposed to APP jets generated by the same plasma system. The distance between the water surface and the bottom end of the plasma system was set at 6 mm and the tip of plasma generated by this system was in contact with the water surface. The applied peak-to-peak voltage was set at 6, 9, or 12 kV and the He flow rate was set at 1 L/min. The pH of plasma-irradiated water was also measured with a pH meter (LAQUAtwinB-711/712, HORIBA).

III. RESULTS

A. Densities of Ions Emitted from the APP Jet System

Figure 3 shows the densities of positive and negative ions in ambient air as functions of distance from the plasma system. The ion densities were measured by an ion counter, as

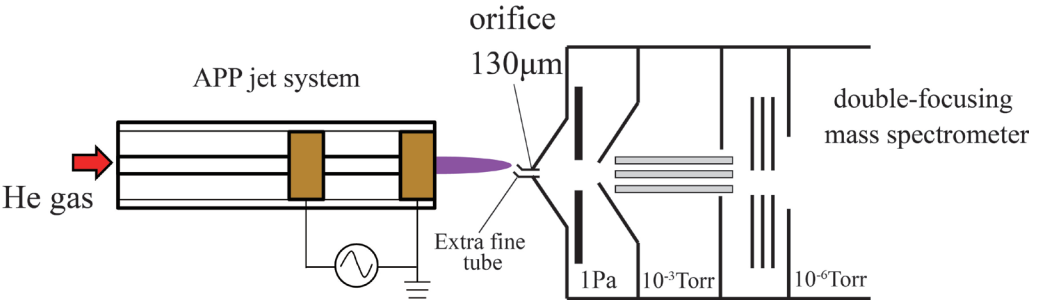

FIG. 2: Schematic diagram of mass spectrometry of ions emitted from the helium-based low-frequency APP jet system. The outside chamber of the mass spectrometer was electrically grounded.

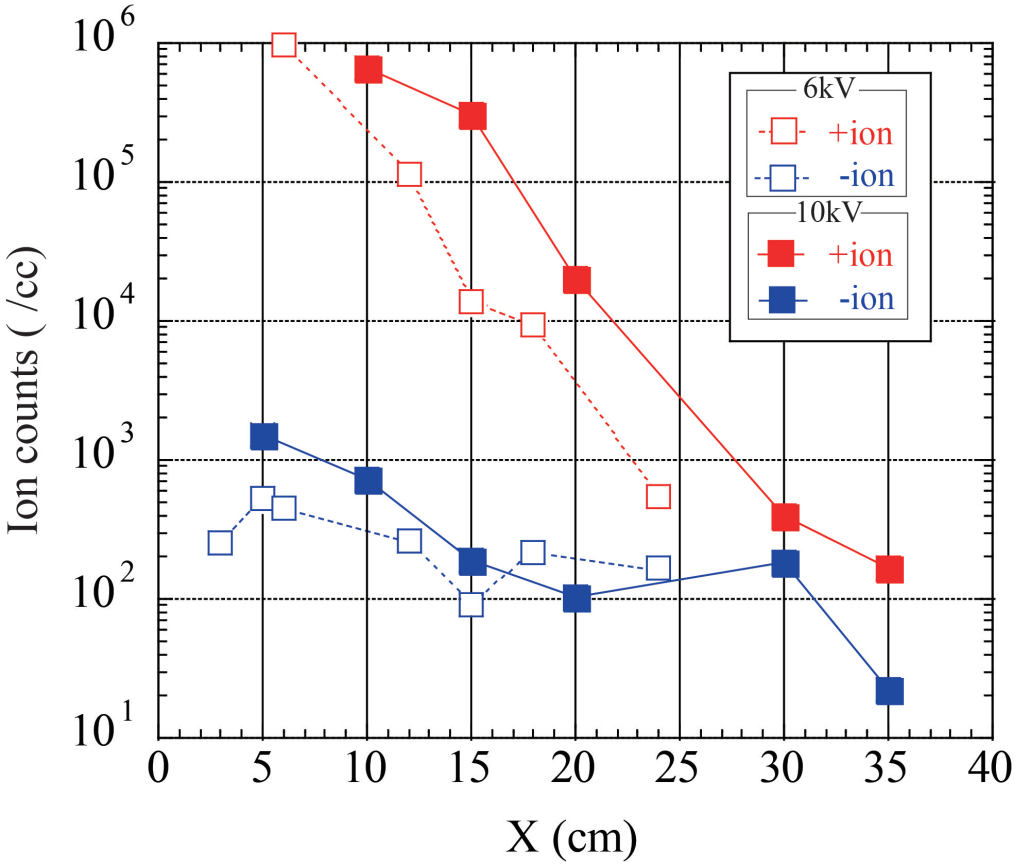

FIG. 3: Densities of negative and positive ions diffused from the low-frequency APP jet system as functions of the position from the plasma along the laboratory bench surface, as shown in Figure 1. The peak-to-peak voltage of the plasma system was set at either 6 or 10 kV, the voltage frequency was about 27 kHz, and the He gas flow rate was 1 L/min.

shown in Figure 1. The peak-to-peak voltage was set at either 6 or 10 kV. The He gas flow rate was 1 L/min. The distance between the laboratory bench and the bottom end of the APP jet system was set at 20 mm, so that the tip of the plasma jet (i.e., the light-emitting region seen in the naked eye) just touched the laboratory bench surface. The spot diameter of the APP jet was less than 1 mm. It may be seen clearly in Figure 3 that ions existed outside of the luminescent part of the plasma and the ion density decreased with a power law as a function of the distance from the plasma. The positive and negative ion densities were over ranged ($>10^6$ cm^{-3}) when the distance was less than 6 and 3 cm, respectively. When there was no plasma (with or without a He gas flow), the density of positive or negative ions was approximately 10^2 cm^{-3}.

As shown in Figure 3, significantly more positive ions than negative ions were observed away from the plasma. This is always the case with this He flow rate, but the negative ion density can be higher than the positive ion density with a different flow rate or under different discharge conditions. The ion density values can significantly vary from day to day even under the same discharge conditions, possibly depending on the humidity and other environmental conditions. Therefore, the data shown in Figure 3 should be construed only as an example of ion density profiles measured around the plasma system.

B. Mass Spectrometry of Negative Ions Originating from APP Jets

Mass spectrometry of negative and positive ions emitted from the APP jet system was also performed. Figure 4 shows peaks of the observed negative ions. The peak-to-peak voltage was 9 kV and the He gas flow rates were 2 L/min and (b) 3 L/min. Assignment of mass spectrum peaks are given in the figure and in Table 1. Nearly all peaks have been assigned except for the peaks at the mass-to-charge ratios of m/z= 56, 74, and 91, which may arise from some impurities. Ions in the shaded area cannot be identified in this mass spectrometry system, as mentioned in the previous section. It is also known that no O_3^- can be detected by this mass spectrometry system; it has been confirmed that externally supplied O_3^- ions are converted to HO_2^- ions inside of this system. Therefore, no peak was assigned to O_3^- or a water cluster that contains O_3^-.

The largest peak in both Figure 4a and Figure 4b is at m/z = 44, which may be assigned to CO_2^- or N_2O^-. Because the electron affinity of CO_2 is low, CO_2^- is unlikely to be formed by electron attachment directly, but rather may be formed by attachment of O to CO^-. The peak at m/z = 60 may be assigned to CO_3^- or $N_2O_2^-$.[29] Other large peaks include those at m/z = 61 and 77, which may be assigned to HCO_3^-, $CH_3CO^-(H_2O)$, and HCO_4^-, respectively. These negative ions are considered to be formed by the following reactions:

$$HO_2^- + CO_2 + M \rightarrow HCO_4^- + M^{28,30}$$
$$OH^- + CO_2 + M \rightarrow HCO_3^- + M^{31-33}$$

where "M" refers to a molecule associated with the three-body collision. The observation of HCO_3^- is also consistent with that of Bruggeman et al. (2010)[20] for a different

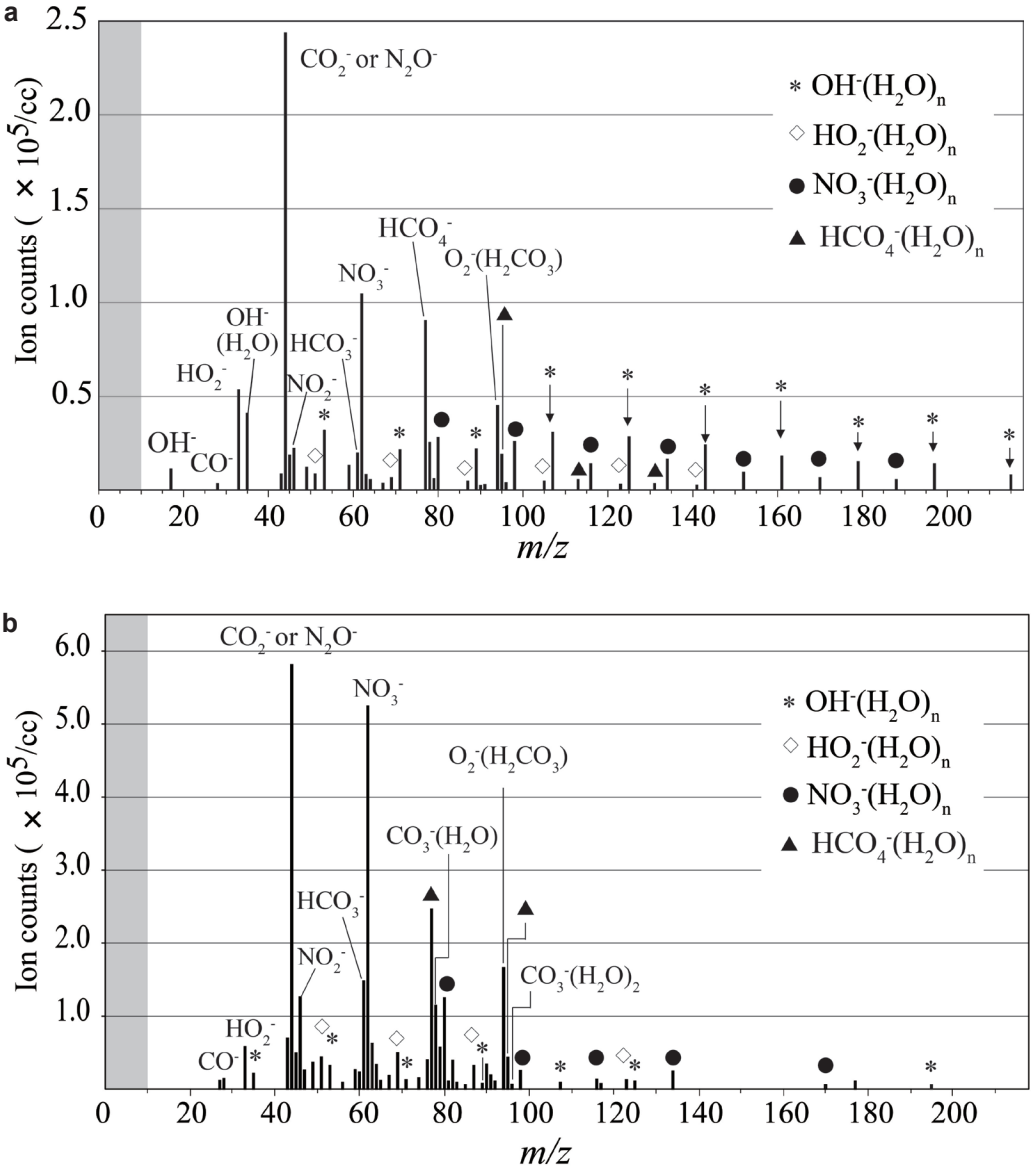

FIG. 4: Mass spectrometry of negative ions emitted from the low-frequency APP jet system shown in Figure 2 with the He gas flow rates of 2 L/min (a) and 3 L/min (b). The horizontal axis represents the mass-to-charge ratio. Because most ions are expected to be singly charged, the horizontal axis practically represents the mass of each ion. The peak-to peak voltage was 9 kV and the voltage frequency was ~27 kHz. Negative ions with masses lower than 10 (i.e., those in the shaded region) cannot be measured in this mass spectrometer.

TABLE 1. Peak Assignments Not Given in Figure 4

m/z	Assignment
27	HCN^-
43	CH_3CO^-
45	HCO_2^- or $HCN^-(H_2O)$
47	$HCO^-(H_2O)$
49	$HNO^-(H_2O)$
59	CH_3COO^-
60	CO_3^- or $N_2O_2^-$
61	HCO_3^- or $CH_3CO^-(H_2O)$
63	$HCO_2^-(H_2O)$ or HNO_3^- or $HCN^-(H_2O)_2$
64	$NO_2^-(H_2O)$
65	$HCO^-(H_2O)_2$
67	$HNO^-(H_2O)_2$
76	CO_4^-
78	$CO_3^-(H_2O)$ or $N_2O_2^-(H_2O)$
79	$HCO_3^-(H_2O)$, $NO_2^-(HO_2)$ or or $CH_3CO^-(H_2O)_2$
81	$HCO_2^-(H_2O)_2$ or $HNO_3^-(H_2O)$ or $HCN^-(H_2O)_3$
82	$NO_2^-(H_2O)_2$
83	$HCO^-(H_2O)_3$
85	$HNO^-(H_2O)_3$
90	$NO_2^-(CO_2)$
92	$NO_2^-(NO_2)$
96	$CO_3^-(H_2O)_2$ or $N_2O_2^-(H_2O)_2$
117	$HCO_2^-(H_2O)_4$ or $HNO_3^-(H_2O)_3$ or $HCN^-(H_2O)_5$

type of helium-based APP.

Ions that have a mass $m/z = 62$ include NO_3^-, $CO_2^-(H_2O)$, and $N_2O^-(H_2O)$. However, based on the discussion on the stability of negative ion water clusters, earlier studies[27,28,31,34,35] on negative corona discharge in air typically assign the peak at $m/z = 62$ to NO_3^-. Therefore, in Figure 4a, we have also assigned the peaks at $m/z = 62 + 18\,n$ with n being an integer to $NO_3^-(H_2O)_n$. Similarly, the peaks at $m/z = 46+18n$ are assigned to $NO_2^-(H_2O)_n$.[27,31,35–37]

It should be noted that no O_2^- peak is shown in Figure 4a or 4b. However, this does not mean that the APP jet system generates no O_2^- ions. Using the same double-focusing mass spectrometer, Sekimoto et al.[28,34] observed $OH^-(H_2O)_n$ and $HO_2^-(H_2O)_n$ ions

generated by their atmospheric-pressure negative corona discharge, but no $O_2^-(H_2O)_n$ ions, as we have reported here with our APP jet system. However, they also observed $O_2^-(H_2O)_n$ ions for the same atmospheric-pressure negative corona discharge with their triple-quadrupole mass spectrometer. One of the essential differences between these double-focusing and triple-quadrupole mass spectrometers is the length of the ion path, especially the orifice capillary connecting the gas inlet and the first differentially pumped stage. Along the ion path, the pressure gradient is the largest in the orifice capillary and some gaseous chemical reactions are most likely to occur there. For example, the lifetime of $O_2^-(H_2O)_n$ is much shorter than other negative ion water clusters such as $OH^-(H_2O)_n$[28,31] and may be lost due to reactions such as:

$$O_2^- + NO_2 \rightarrow NO_2^- + O_2$$[32]
$$O_2^-(H_2O)_n + NO \rightarrow NO_3^- + nH_2O$$[38]

while they travel along the ion path in the mass spectrometer. Therefore, the fact that the mass spectra of Figure 4 do not show the peak for O_2^- ions does not rule out the possibility of O_2^- ion generation by the APP jet system used in this study. These observations indicate that the observed ion mass spectrum for the same discharge could vary from spectrometer to spectrometer.

Large water clusters of $Y^-(H_2O)_n$ with $n \geq 3$ seen in Figure 4 are those with core ions of $Y^- = OH^-$, HO_2^-, NO_3^-, HCO^-, HCO_2^-, HNO^-, HNO_3^-, HCO_4^-, and HCN^-. Earlier studies[28,31,39] with negative corona discharges have also shown that $Y^- = CO_3^-$, HCO_3^-, NO_2^-, NO_3^-, O_2^-, O_3^-, and $NO_2^-(HNO_3)_2$ can also form large ion clusters in large quantities under certain conditions. Ion water clusters of $Y^- = O^-$ were also observed for helium-based discharges in earlier studies,[20,21] although their peak heights (and therefore their relative abundances) were very low. It should be noted that, in acidic conditions, CO_3^-, HCO_3^-, and HCO_4^- ions dissolved into water are almost entirely converted to CO_2 and hardly remain as carbonate ions in water.

Water molecules that are attached directly to the core ion via Coulomb interaction between the ion charge and the dipole moment of each water molecule are said to form the first hydrated shell. The number of water molecules that can form the first hydrated shell depends on the ion species. For example, the first hydrated shell of $O_2^-(H_2O)_n$ is considered to be at $n = 4$.[40–42] Water molecules attached to the outside of the first hydrated shell are considered to do so via intermolecular forces and therefore extremely weakly bound. Therefore, such large ion water clusters beyond the first hydrated shells can exist only in nearly collisionless conditions.

The pressure in the first differentially pumped stage of the mass spectrometer used in this study was ~1 Torr and the large difference in pressure between the outside and this stage causes an adiabatic expansion of the gas flowing into the mass spectrometer chamber. Adiabatic expansion promotes the formation of gas clusters, especially those of ions with water molecules.[27] Large ion water clusters beyond the first hydrated shells may be formed in the low-pressure and nearly collisionless region as ion clusters travel from the first differentially pumped stage through the second (10^{-3} Torr) and third (10^{-6} Torr) dif-

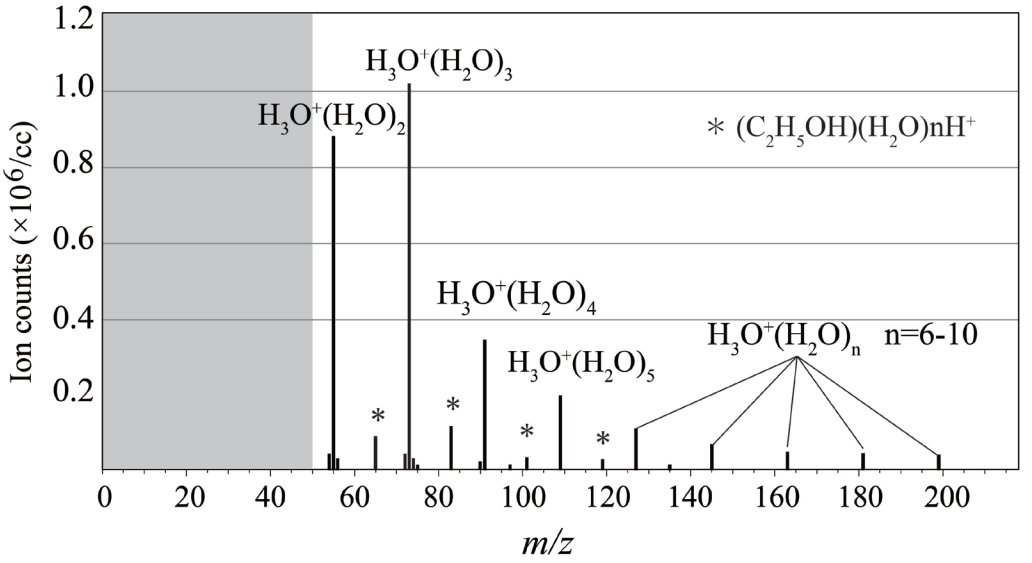

FIG. 5: Mass spectrometry of positive ions emitted from the low-frequency APP jet system shown in Figure 2. The He gas flow was 3 L/min, the peak-to peak voltage was 9 kV, and the voltage frequency was ~27 kHz. Positive ions with masses lower than 50 (i.e., those in the shaded region) cannot be measured in this mass spectrometer.

ferentially pumped stages to the mass spectrometer. Therefore, large ion water molecules observed in mass spectra of Figure 4 should not be construed to exist in ambient air.

Small ion water clusters within the first hydrated shell may be formed in ambient air if the humidity is sufficiently high. For example, when APP jets are applied to a water surface, the density of water molecules is typically high near the water surface and small ion water clusters may be formed there. Furthermore, such water clusters are likely to dissolve directly into water as they reach the water surface.

C. Mass Spectrometry of Positive Ions Originating from APP Jets

Figure 5 shows all positive ions observed by mass spectrometry originating from the same helium-based APP jets. The discharge conditions are the same as those of Figure 4b. No ions can be identified in the shaded region of Figure 5 by the mass spectrometer used in this study. The dominant peaks in Figure 5 represent hydronium ion[43] water clusters $H_3O^+(H_2O)_n$. Positive ion peak at $m/z = 65$ may be assigned to the protonated ethanol molecule $(C_2H_5OH)(H_2O)H^+$ derived from ethanol molecules that were inadvertently present in ambient air. Other small peaks have not been identified. The observation that the only large positive ion clusters are $H_3O^+(H_2O)_n$ is consistent with those of earlier studies based on positive corona discharges,[44] as well as nearly all other discharges generated by different ionization methods.[20,21,45–49]

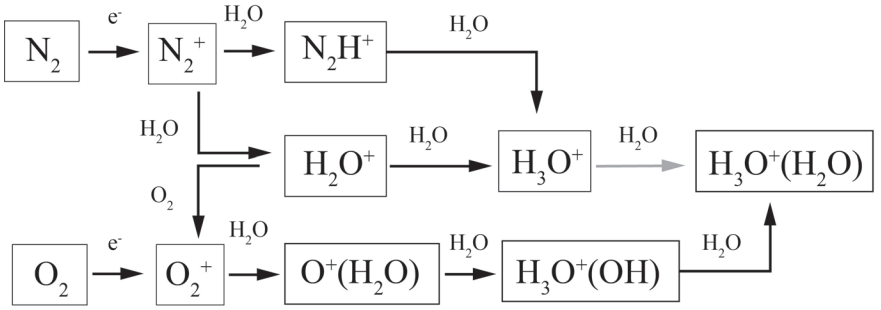

FIG. 6: Reaction chains of positive ions in humid air proposed by Sekimoto et al.[50] According to this scheme, electron impact ionizations in air generate nitrogen and oxygen molecular ions and, through a series of reactions (a–k) given in the Materials and Methods, they eventually form water clusters of hydronium ions.

The series of gas-phase reactions involving positive ions are indeed known to lead to $H_3O^+(H_2O)_n$ as the final products. Figure 6 summarizes the reaction chains arising from a discharge in humid air proposed by Sekimoto and Takayama (2011)[50] based on the following chemical reactions:

(a) $N_2 + e^- \rightarrow N_2^+ + 2e^-$ [electron impact ionization]
(b) $N_2^+ + H_2O \rightarrow N_2H^+ + OH$[44]
(c) $N_2^+ + H_2O \rightarrow H_2O^+ + N_2$[44]
(d) $N_2H^+ + H_2O \rightarrow H_3O^+ + N_2$[51]
(e) $H_2O^+ + O_2 \rightarrow O_2^+ + H_2O$[51]
(f) $H_2O^+ + H_2O \rightarrow H_3O^+ + OH$[51]
(g) $H_3O^+ + H_2O + M \rightarrow H_3O^+(H_2O) + M$ with M=N_2, O_2[44]
(h) $O_2 + e^- \rightarrow O_2^+ + 2e^-$ [electron impact ionization]
(i) $O_2^+ + H_2O + M \rightarrow O_2^+(H_2O) + M$ with M = N_2, O_2[51]
(j) $O_2^+(H_2O) + H_2O \rightarrow H_3O^+ + HO + O_2 \rightarrow H_3O^+(HO) + O_2$[52]
(k) $H_3O^+(HO) + H_2O \rightarrow H_3O^+(H_2O) + OH$[52]

It may also be seen that many OH radicals are produced in these reaction paths (numbers shown in brackets).

It is known that the hydronium ion water cluster with the full first hydrated shell is $H_3O^+(H_2O)_3$. Therefore, larger ion water molecules in the spectrum of Figure 5 were likely to be generated in the mass spectrometer chamber. The stability of $H_3O^+(H_2O)_n$ and reaction paths of Figure 6 suggest that all positive ions generated by a discharge in ambient air may be considered to dissolve into water as hydronium ion (or H^+ in an abbreviated expression).

D. Concentrations of Reactive Species in Pure Water Exposed to App Jets

As we have seen in the preceding subsection, OH radicals are generated in a series of

chemical reactions, leading to the formation of $H_3O^+(H_2O)_n$. It is known that hydroxyl radicals typically form H_2O_2 in both the gas and liquid phases.[19,53–55] To confirm how our helium-based low-frequency APP jet system generates some reactive species in pure water, we measured the concentrations of H_2O_2 and NO_2^- in pure water exposed to APP jets generated by the same plasma system.

Figure 7 shows the increase of the concentrations of H_2O_2 and NO_2^- in water as the function of the APP exposure time at different applied peak-to-peak applied voltages. It may be seen that the H_2O_2 and NO_2 concentrations in 2 ml of pure water increased linearly with the APP jet irradiation time. The H_2O_2 concentrations observed here are consistent with the observation in an earlier study of a similar experiment with the same plasma system.[19]

IV. CONCLUSIONS

We have performed mass spectrometry for ions generated by helium-based low-frequency APP jets in ambient air. It is known that mass spectra obtained from an APP source may vary, depending on the mass spectrometry system, as various ions are lost or generated in the differentially pumped stages in the mass spectrometry system. In other words, the design of the ion path from the orifice to the mass spectrometer sensitively affects the observed mass spectra. Given this fact, the ion mass spectra that we obtained in this study for our APP jet system are consistent with those of the earlier study by Oh et al. (2011)[21] using a similar helium-based APP jets. Indeed, the observed ions originating from the APP jet system used in this study are qualitatively similar to those obtained from other discharges, including corona discharges[27,28,31,34,50] and RF-driven atmospheric-pressure glow discharge[20] with some humidity.

For positive ions, regardless of how an APP is generated, the final dominant ion products are hydronium ions and their ion water clusters $H_3O^+(H_2O)_n$. If a water surface is exposed to such plasma, all positive ions that remain in water should be hydronium ions H_3O^+ (or H^+ in an abbreviated expression) because other positive ions are much less stable in the presence of water molecules, as suggested by the reaction paths of Figure 6. Similarly, for negative ions, only a small number of kinds of negative ions stably form dominant water clusters. Because carbonic acid is mostly likely to be converted to CO_2 under typical conditions of water irradiated by APPs, the dominant-negative ions that may exist most stably in water are NO_2^-, NO_3^-, and OH^- when the water is exposed to an APP. Other negative ions, such as O_2^-, HO_2^-, and O_3^-, are also likely to dissolve into water, but they are known to be highly reactive in water and may be quickly converted to other species due to their aqueous chemical reactions. The obtained mass spectra in the gas phase also suggest that, when an APP jets is applied to a wet surface (such as living tissues in therapeutic applications of plasmas), ion water clusters are likely to be formed near the surface, where the humidity is expected to be high. The mass spectrometry data obtained in this study indicate that all dominant ion species generated by the APP jet system contain either oxygen or nitrogen, which suggests that the plasma also generate a large amount of (charge neutral) RONS.

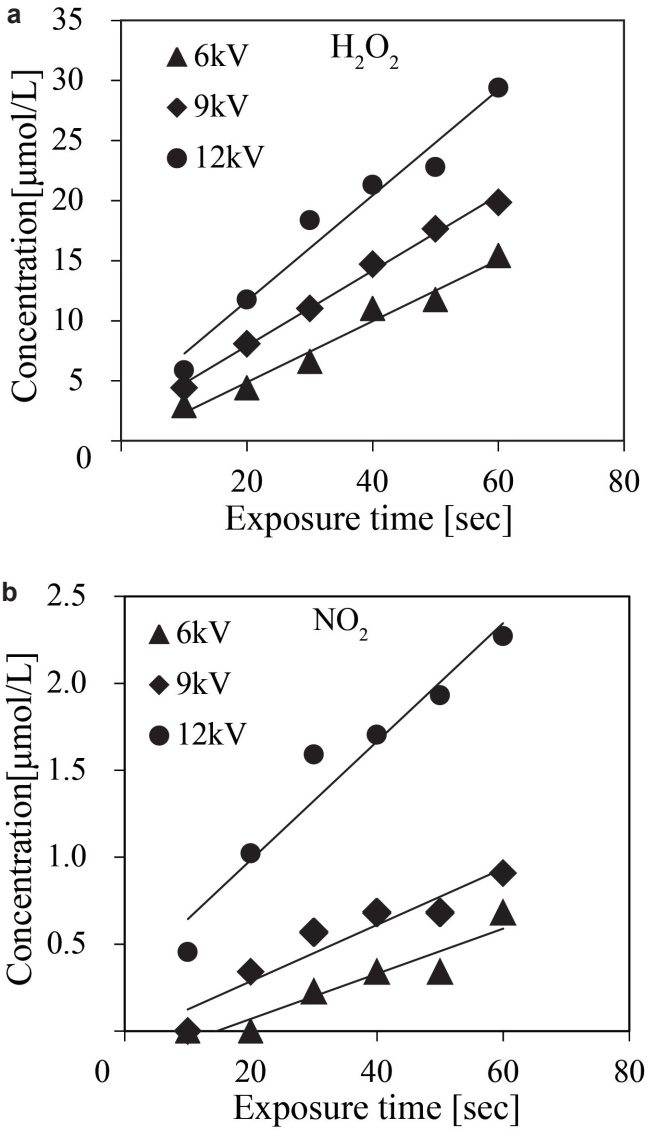

FIG. 7: The concentrations of H_2O_2 (a) and NO_2 (b) in 2 ml of pure water exposed to APP jets generated by the same plasma system as that shown in Figure 1. The tip of the plasma was in contact with the water surface. The horizontal axis represents the plasma irradiation time. The peak-to-peak voltage of the plasma system was set at 6, 9, or 12 kV; the voltage frequency was approximately 27 kHz; and the He flow rate was set at 1 L/min. The concentration measurements were performed by colorimetry with 4-aminoantipyrine for H_2O_2 (a) and naphthyl ethylenediamine for NO_2^- (b). The pH of the water was not controlled but remained within the range at which the above colorimetry method might be applied.

To characterize the APP jet system used in this study, we also measured positive and negative ion densities away from the plasma system using an ion counter. Although ions generated by the plasma system can exist away from the plasma, their densities decrease exponentially away from the plasma.

The concentrations of H_2O_2 and NO_2^- in water exposed to the same plasma were also measured with a colorimetric method. These results indicate that the origins of H_2O_2 and NO_2^- in the water are RONS generated by the plasma. Although mass spectrometry is, in general, so sensitive that it can detect very small quantities of gaseous ions, the observation shows that the concentrations of RONS generated by the plasma in the gas phase or at the gas–water interface are sufficiently high that they can affect the chemical nature of water exposed to the plasma.

ACKNOWLEDGMENTS

This work was partially supported by a Grant-in-Aid for Scientific Research from the Japan Society for the Promotion of Science (JSPS)/MEXT. The authors thank Dr. Eizo Murakami of Asahi Kogyosha and Dr. Yoshimi Suyama of Hazama Ando for useful discussions and technical support in the ion-counting experiments Dr. Kazumasa Ikuse of Osaka University for insightful discussions on chemical reactions in water.

REFERENCES

1. Fridman G, Friedman G, Gutsol A, Shekhter AB, Vasilets VN, Fridman A. Applied plasma medicine. Plasma process Polym. 2008;5:503–33.
2. Stoffels E, Sakiyama Y, Graves D. Cold atmospheric plasma: charged species and their interactions with cells and tissues. IEEE Trans Plasma Sci. 2008;36:1441–57.
3. Laroussi M, Kong MG, Morfill G, Stolz W. Plasma medicine: applications of low-temperature gas plasmas in medicine and biology. Cambridge: Cambridge University Press; 2012.
4. Fridman A, Friedman G. Plasma medicine. Hoboken, NJ: Wiley; 2013.
5. Graves J. The emerging role of reactive oxygen and nitrogen species in redox biology and some implications for plasma applications to medicine and biology. J Phys D: Appl Phys. 2012;45:263001–42.
6. Park G, Lee H, Kim G, Lee JK. Global model of He/O_2 and Ar/O_2 atmospheric pressure glow discharges. Plasma Process Polym. 2008;5:569–76.
7. Liu DX, Bruggeman P, Iza F, Rong MZ, Kong MG. Global model of low-temperature atmospheric-pressure He + H_2O plasmas. Plasma Sources Sci. Technol. 2010;19:025018–39.
8. Liu DX, Iza F, Wang XH, Kong MG, Rong MG. He+O_2+H_2O plasmas as a source of reactive oxygen species. Appl Phys Lett. 2011;98:221501–3.
9. Murakami T, Niemi K, Gans T, O'Connell D, Graham WG. Chemical kinetics and reactive species in atmospheric pressure helium–oxygen plasmas with humid-air impurities. Plasma Sources Sci Technol. 2013;22:015003–31.
10. Murakami T, Niemi K, Gans T, O'Connell D, Graham WG. Interacting kinetics of neutral and ionic species in an atmospheric-pressure helium–oxygen plasma with humid air impurities. Plasma Sources Sci Technol. 2013;22:045010–21.

11. Murakami T, Niemi K, Gans T, O'Connell D, Graham WG. Afterglow chemistry of atmospheric-pressure helium–oxygen plasmas with humid air impurity. Plasma Sources Sci Technol. 2014;23:025005–16.
12. Tian W, Kushner MJ. Atmospheric pressure dielectric barrier discharges interacting with liquid covered tissue. J Phys D: Appl Phys. 2014;47:165201–21.
13. Yagi I, Ono R, Oda T, Takaki K. Two-dimensional LIF measurements of humidity and OH density resulting from evaporated water from a wet surface in plasma for medical use. Plasma Sources Sci Technol. 2015;24:015002–9.
14. Tian W, Kushner MJ. Long-term effects of multiply pulsed dielectric barrier discharges in air on thin water layers over tissue: stationary and random streamers. J Phys D: Appl Phys. 2015;48:494002–19.
15. Ando A, Uno H, Uris T, Hamaguchi S. Grid-pattern formation of extracellular matrix on silicon by low-temperature atmospheric-pressure plasma jets for neural network biochip fabrication. Appl Surf Sci. 2013;276:1–6.
16. Ando A, Asano T, Urisu T, Hamaguchi S. Micro-pattern formation of extracellular matrix (ECM) layers by atmospheric-pressure plasmas and cell culture on the patterned ECM. J Phys D: Appl Phys. 2011;44:482002–6.
17. Ando A, Asano T, Sayed MA, Tero R, Kitano K, Urisu T, Hamaguchi S. Extracellular matrix patterning for cell alignment by atmospheric pressure plasma jets. Jpn J Appl Phys. 2012;51:036201–7.
18. Ikawa A, Kitano K, Hamaguchi S. Effects of pH on bacterial inactivation in aqueous solutions due to low-temperatureatmospheric pressure plasma application. Plasma Process Polym. 2010;7:33–42.
19. Miura T, Ando A, Hirano K, Ogura C, Kanazawa T, Ikeguchi M, Seki A, Nishihara S, Hamaguchi S. Proliferation assay of mouse embryonic stem (ES) cells exposed to atmospheric-pressure plasmas at room temperature. J Phys D: Appl Phys. 2014;47:445402–13.
20. Bruggeman P, Iza F, Lauwers D, Aranda-Gonzalvo Y. Mass spectrometry study of positive and negative ions in a capacitively coupled atmospheric pressure RF excited glow discharge in He–water mixtures. J Phys D: Appl Phys. 2010;43:012003–8.
21. Oh JS, Aranda-Gonzalvo Y, Bradley JW. Time-resolved mass spectroscopic studies of an atmospheric-pressure helium microplasma jet. J Phys D: Appl Phys. 2011;44:365202–11.
22. Dünnbier M, Schmidt-Bleker A, Winter J, Wolfram M, Hippler R, Weltmann KD, Reuter S. Ambient air particle transport into the effluent of a cold atmospheric-pressure argon plasma jet investigated by molecular beam mass spectrometry. J Phys D: Appl Phys. 2013;46:435203–11.
23. Oh JS, Furuta H, Hatta A, Bradley JW. Investigating the effect of additional gases in an atmospheric-pressure helium plasma jet using ambient mass spectrometry. Jpn J Appl Phys. 2015;54:01AA03 1–5.
24. Kitano K, Aoki H, Hamaguchi S. Radio-frequency-driven atmospheric-pressure plasmas in contact with liquid water. Jpn J Appl Phys. 2006;45:8294.
25. Aoki H, Kitano K, Hamaguchi S. Plasma generation inside externally supplied Ar bubbles in water. Plasma Sources Sci Technol. 2008;17:025006–11.
26. Sekimoto K and Takayama M. Effects of H_3O+, $OH-$, O_2- , NO_x- and NO_x for Escherichia coli inactivation in atmospheric pressure DC corona discharges. J Phys D: Appl Phys. 2015; 48:305401–9.
27. Sekimoto K, Takayama M. Influence of needle voltage on the formation of negative core ions

using atmospheric pressure corona discharge in air. Int J Mass Spectrom. 2007;261:38–44.
28. Sekimoto K, Takayama M. Observations of different core water cluster ions $Y^-(H_2O)_n$ (Y = O_2, HO_x, NO_x, CO_x) and magic number in atmospheric pressure negative corona discharge mass spectrometry. Int J Mass Spectrom. 2011;46:50–60.
29. Sabo M, Páleník J, Kučera M, Han H, Wang H, Chu Y, Matejčík S. Atmospheric pressure corona discharge ionisation and ion mobility spectrometry/mass spectrometry study of the negative corona discharge in high purity oxygen and oxygen/nitrogen mixtures. Int J Mass Spectrom. 2010;293:23–27.
30. McAllister T, Nicholson AJC, Swingler DJ. Negative ions in the flame ionization detector and the occurrence of HCO_4^-. Int J Mass Spectrom Ion Phys. 1978;27:43–48.
31. Nagato K, Matsuib Y, Miyatab T, Yamauchib T. An analysis of the evolution of negative ions produced by a corona ionizer in air. Int J Mass Spectrom, 2006;248:142–47.
32. Fehsenfeld FC, Ferguson EE. Laboratory studies of negative ion reactions with atmospheric trace constituents. J Chem Phys. 1974;61:3181–93.
33. Skalny JD, Orszagh J, Mason NJ, Rees JA, Aranda-Gonzalvo Y, Whitmore TD. Mass spectrometric study of negative ions extracted from point to plane negative corona discharge in ambient air at atmospheric pressure. Int J Mass Spectrom. 2008;272:12–21.
34. K. Sekimoto, K. Kikuchi, and M. Takayama. Temperature dependence of magic number and first hydrated shell of various core water cluster ions $Y^-(H_2O)_n$ (Y = O_2, HO_x, NO_x, CO_x) in atmospheric pressure negative corona discharge mass spectrometry. Int J Mass Spectrom. 2011;306:44–50.
35. Skalny JD, Mikoviny T, Matejcik S, Mason NJ. An analysis of mass spectrometric study of negative ions extracted from negative corona discharge in air. Int J Mass Spectrom. 2004;233:317–24.
36. Shahin MM. Nature of charge carriers in negative coronas. Appl Opt Suppl Electrophotogr. 1969;3:106–110.
37. Gravendeel B, de Hoog FJ. Clustered negative ions in atmospheric negative corona discharges in the Trichel regime. J Phys B: At Mol Phys. 1987;20:6337–61.
38. Adams NG, Bohme DK, Dunkin DB, Fehsenfeld FC, Ferguson EE. Flowing afterglow studies of formation and reactions of cluster ions of O_2^+, O_2^-, and O^-. J Chem Phys. 1970;52:3133–40.
39. Sabo M, Okuyama Y, Kučera M, Matejčík S. Transport and stability of negative ions generated by negative corona discharge in air studied using ion mobility-oaTOF spectrometry. Int J Mass Spectrom. 2013;334:19–26.
40. Weber JM, Kelley JA, Nielsen SB, Ayotte P, Johnson MA. Isolating the spectroscopic signature of a hydration shell with the use of clusters: superoxide tetrahydrate. Science. 2000;287:2461–63.
41. Weber JM, Kelly JA, Robertson WH, Johnson MA. Hydration of a structured excess charge distribution: infrared spectroscopy of the $O_2^-\cdot(H_2O)_n$, ($1 \le n \le 5$) clusters. J Chem Phys. 2001;114:2698–706.
42. Seta T, Yamamoto M, Nishioka M, Sadakata M. Structures of hydrated oxygen anion clusters: DFT calculations for $O^-(H_2O)_n$, $O_2^-(H_2O)_n$, and $O_3^-(H_2O)_n$ (n = 0–4). J Chem Phys. 2003;107:962–67.
43. Eigen M. Proton transfer, acid-base catalysis, and enzymatic hydrolysis. Part I: Elementary processes. Angew Chem Internat Edit. 1964;3:1–19.
44. Pavlik M, Skalny JD. Generation of $[H_3O]^+\cdot(H_2O)_n$ clusters by positive corona discharge in

air. Rapid Commun Mass Spectrom. 1997;11:1757–66.
45. Lin SS. Detection of large water clusters by a low rf quadrupole mass filter. Rev Sci Instrum. 1973;44:516–17.
46. Searcy JQ, Fenn JB. Clustering of water on hydrated protons in a supersonic free jet expansion. J Chem Phys. 1974;61:5282–88.
47. Schlosser G, Takáts Z, Vékey K. Formation of solvated ions in the atmospheric interface of an electrospray ionization triple-quadrupole mass spectrometer. J Mass Spectrom. 2003;38:1245–51.
48. König S, Fales HM. Formation and decomposition of water clusters as observed in a triple quadrupole mass spectrometer. J Am Soc Mass Spectrom. 1998;9:814–22.
49. Nagashima U, Shinohara S, Nishi N, Tanaka H. Enhanced stability of ion–clathrate structures for magic number water clusters. J Chem Phys. 1097;84:209–14.
50. Sekimoto K, Takayama M. Study of ion formation and evolution in ambient corona discharge [in Japanese]. Earozoru Kennkyu. 2011;26:203–13.
51. Anicich VG. Evaluated bimolecular ion-molecule gas phase kinetics of positive ions for use in modeling planetary atmospheres, cometary comae, and interstellar clouds. J Phys Chem Ref Data. 1993;22:1469–569.
52. Albritton DL. Ion-neutral reaction-rate constants measured in flow reactors through 1977. Atmo Data Nucl Tab. 1978;22:1–90.
53. Winter J, Wende K, Masur K, Iséni S, Dünnbier M, Hammer MU, Tresp H, Weltmann KD, Reuter S. Feed gas humidity: a vital parameter affecting a cold atmospheric-pressure plasma jet and plasma-treated human skin cells. J Phys D: Appl Phys. 2013;46:295401–11.
54. Winter J, Tresp H, Hammer MU, Iséni S, Kupsch S, Schmidt-Bleker A, Wende K, Dünnbier M, Masur K, Weltmann KD, Reuter S. Tracking plasma generated H_2O_2 from gas into liquid phase and revealing its dominant impact on human skin cells. J Phys D: Appl Phys. 2014;47:285401–13.
55. Wende K, Williams P, Dalluge J, Van Gaens W, Aboubakr H, Bischof J, von Woedtke T, S. Goyal M, Weltmann KD, Bogaerts A, Masur K, Bruggeman PJ. Identification of the biologically active liquid chemistry induced by a nonthermal atmospheric pressure plasma jet. Biointerphases. 2015;10:029518-1-16.